JOURNAL OF MATERIALS SCIENCE 20 (1985) 2757–2766

Stability and work hardening of an Fe–12Cr–23Mn austenitic steel

M. T. JAHN*, C. M. FAN, C. M. WAN
Department of Materials Science and Engineering, National Tsing Hua University, Hsinchu, Taiwan

The effect of pre-strain on the strain-induced martensitic transformation of an Fe–12Cr–23Mn austenitic steel has been investigated through transmission electron microscopy and X-ray analysis. Pre-strain was performed either at room temperature or at 200° C. Final strain was carried out at liquid-nitrogen temperature. The ϵ phase was shown to form on {1 1 1} planes of the austenite matrix predominantly by overlapping of stacking faults. The martensite transformation sequence was $\gamma \rightarrow \epsilon \rightarrow \alpha$. Nucleation of the α phase mainly occurred at intersections of ϵ bands. Austenite stability was shown to increase by pre-strain at 25° C or 200° C. Pre-strain at 200° C has a greater effect on austenite stability than does pre-strain at 25° C. The mechanism was discussed in terms of martensite transformation rate and various substructures introduced during straining. Work hardening was shown to depend on the degree of pre-strain and final strain. The correlation between work hardening and substructures introduced during straining was examined.

1. Introduction

Application of stainless steels, AISI 300 series, has been widely accepted in industry owing to their excellent combination of strength, elongation, toughness and corrosion resistance. Since the alloying elements, nickel and chromium, contained in stainless steels are strategically important and very expensive, many studies have been done to explore the possibility of the substitution of manganese and aluminium for nickel and chromium. Test results identified aluminium and silicon as potential substitutes for chromium to give oxidation and corrosion resistance [1]. Manganese has been chosen as a substitute for nickel because manganese is an austenite stabilizer and can increase the ductility and toughness of alloy steels [2, 3]. Partial phase diagrams and mechanical properties of various Fe–Al–Mn alloy steels were investigated [4–6]. Recently, for use in seagoing ship propellers Wang and Beck [7] discussed the Fe–30Mn–10Al–Si composition as a new stainless steel without nickel or chromium which has good resistance to marine corrosion

The strain-induced austenite → martensite transformations have received considerable attention in 18/8 type stainless steel [8, 9], Fe–Ni systems [9], Fe–Mn and Fe–Mn–Cr–C systems [10]. Several investigations [11, 12] suggested that intersections of shear bands played an important role in nucleating martensite, but dislocation cells, mechanical twins and grain boundaries could inhibit martensite growth. Thus, small prior austenite strain will increase the number of martensite nucleation sites and larger amounts of pre-strain can inhibit martensite transformation. The martensitic transformation from γ (f c c) to α (b c c) phase in some metastable austenitic alloys is rather complicated because of the presence of martensitic ϵ (h c p) phase [13–15]. Using transmission electron microscopy (TEM), Mangonon [11] and Kelly [14] observed that α was nucleated from the ϵ phase. On the other hand, Dash and Otte [13] believed that ϵ forms only because

*Visiting Professor, Department of Mechanical Engineering, California State University, Long Beach, California, USA.

0022–2461/85 $03.00 + .12

of the large shape deformation due to the $\gamma \rightarrow \alpha$ transformation.

Although the effects of strain on change in microstructure and martensitic transformation in Fe–Cr–Ni austenitic steels (conventional stainless steels) have been intensively explored, no similar study has been applied to the Fe–12Cr–23Mn system, which offers the possibility of manganese substitution for nickel. In this study, we used TEM and X-ray techniques to investigate the effects of various austenite prior strains on the change in microstructure and martensitic transformation process during cold working in the Fe–12Cr–23Mn system.

In order to understand the mechanical properties of this new system, austenite stability and correlated hardness of this alloy were examined. It is our hope that a better understanding of $\gamma \rightarrow \epsilon \rightarrow \alpha$ transformation and the correlation between strain hardening and austenite stability of this alloy system will thus be obtained.

2. Experimental details

The chemical composition of the alloy steel investigated in this study was Fe–23Mn–11.58Cr–1.5Si–0.6Al–0.11N. The content of carbon, sulphur or phosphorus was less than 0.03%. The alloy was prepared by induction melting of the appropriate proportions of commercially pure (99.9%) alloy elements in an argon atmosphere. The ingot was forged to 67% reduction in thickness at 1150° C to break up the cast structure, and then homogenized for 24 h at 1150° C. The homogenized plate was cold-rolled, annealed at 950° C, cold-rolled to final thickness and then annealed again at 950° C for 2 h. The dimensions of these as-annealed specimens were 0.3 cm x 3 cm x 10 cm. After each heat treatment the material was quenched in water and then pickled to remove the scale produced during heat treating. The phase is full austenite under the as-annealed condition.

The thermomechanical processes to which the specimens were subjected were divided into three categories:

(a) as-annealed → rolled at elevated temperature (200° C) to 20 or 40% thickness reduction (prior strain) → rolled at −196° C to 5, 10, 15 or 30% thickness reduction (final strain);

(b) as-annealed → rolled at room temperature to 20 or 40% thickness reduction (prior strain) → rolled at −196° C to 5, 10, 15 or 30% thickness reduction (final strain);

(c) as-annealed → rolled at −196° C to 5, 10, 15 or 30% reduction in thickness (no prior strain, only final strain was performed).

A Rockwell-A scale hardness test was carried out to investigate the effect of prior strain on strain hardening rate. Examination of microstructure was performed by optical and transmission electron microscopy. The etchant for optical microscopy was $HNO_3 + HCl + CH_3COOH + H_2O$ in volume ratio 10:15:10:65. The thin foil for TEM was obtained by a jet method. The electropolishing solution was $HClO_4 + CH_3COOH$ (6:94). The voltage was 12 to 18 V and polishing was at room temperature. Observation of the foil was done with a JEOL 100-B TEM operating at 100 kV. Pictures of bright-field, dark-field and selected area diffraction patterns were taken to analyse the microstructures. The martensitic phase transformation was examined by both TEM and X-ray techniques. A Shimadzu X-ray diffractometer equipped with filtered Mo$K\alpha$ radiation was used. The relative integrated intensities of peaks corresponding to the γ, ϵ and α phases were compared and the volume fractions of martensite phases (ϵ and α) calculated. The method assumed a random orientation. Any preferred orientation would introduce some errors. The data obtained from the X-ray technique were for qualitative analysis only.

3. Experimental results

3.1. ϵ (hcp) and α (bcc) martensitic transformation

Fig. 1 shows the TEM microstructure in an as-annealed specimen. The grain size was about 3.0 μm. The phase was full austenite. Some specimens were quenched from the annealing

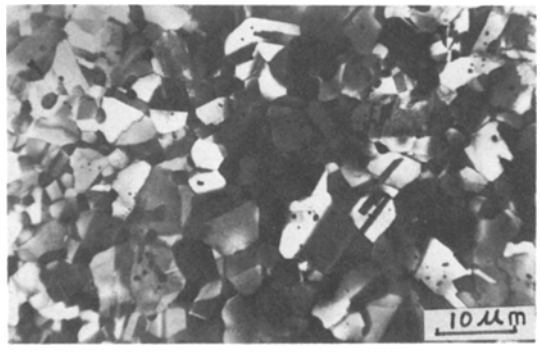

Figure 1 TEM microstructure of an as-annealed specimen.

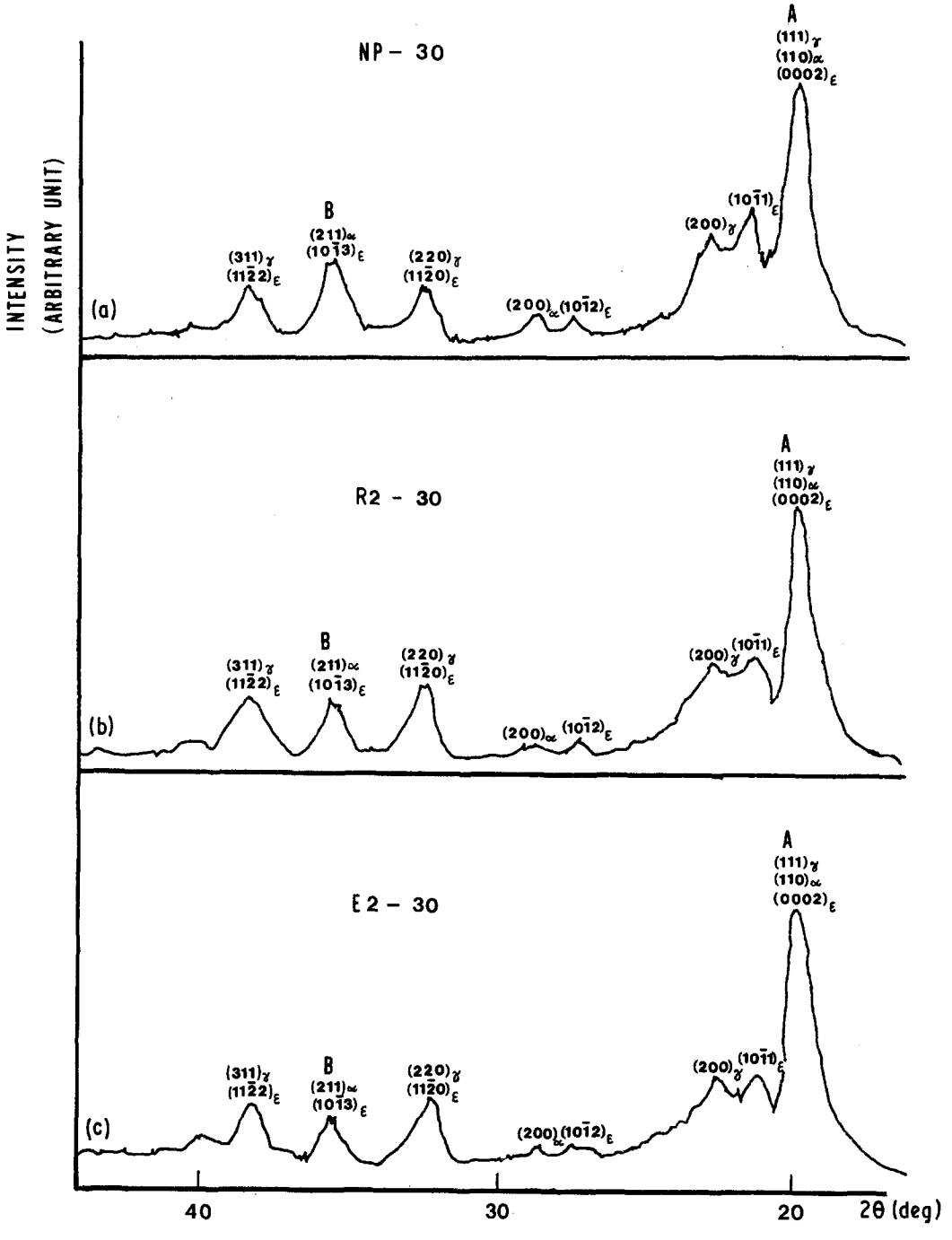

Figure 2 X-ray diffractometer pattern of specimen (a) with 0% prior strain and 30% final strain, (b) with 20% prior strain (at 25° C) and 30% final strain, and (c) with 20% prior strain (at 200° C) and 30% final strain.

temperature (950° C) directly to liquid-nitrogen temperature (−196° C). No ϵ or α martensite was observed in these as-quenched specimens. It was evident that M_s (the temperature at which the martensite transformation starts spontaneously on cooling) of the alloy investigated was below −196° C. Both X-ray analysis and TEM observation showed evidence of ϵ transformation in specimens deformed at −196° C. X-ray analysis indicated the presence of $10\bar{1}1$, $10\bar{1}2$ and $11\bar{2}0$ reflections, which are typical of the ϵ (h c p) structure, as shown in Fig. 2. The results of the

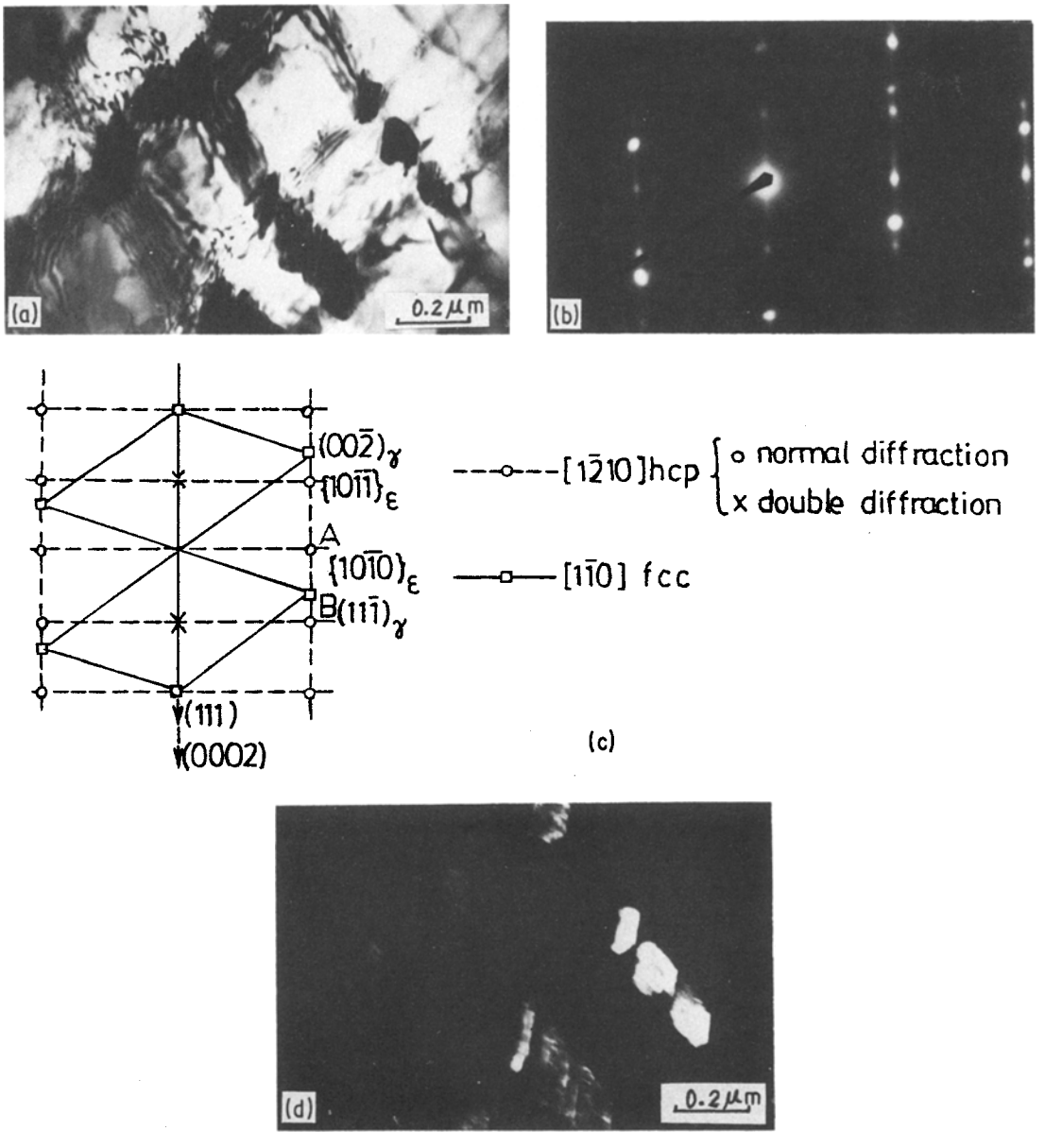

Figure 3 TEM microstructure of a specimen with 0% prior strain and 10% final strain: (a) bright-field image; (b) diffraction pattern taken at centre of (a); (c) indexed diffraction pattern; (d) dark-field image due to spot A.

TEM investigations are illustrated in Fig. 3. These results confirm further that the ϵ phase is h c p and that stacking faults play an important role in the martensite transformation. The electron diffraction pattern, Fig. 3b, taken at the central area of Fig. 3a is schematically drawn and indexed in Fig. 3c. Fig. 3d is the dark-field image due to reflection of spot A $\{1\,0\,\bar{1}\,0\}$(see Fig. 3c). Further investigation indicated that more deformation (at -196° C) produced more overlapping of stacking faults, which resulted in the increase of ϵ nuclei.

In no case was the α phase observed without the formation of the ϵ phase. The amount of ϵ phase observed in our study was always much larger than the amount of α martensite. As shown in Fig. 2, peaks of $(2\,0\,0)_\alpha$ and $(2\,1\,1)_\alpha$ were found in specimens with a final strain of 30% by X-ray analysis. Fig. 4, obtained by TEM microscopy of a specimen having no prior strain but with a

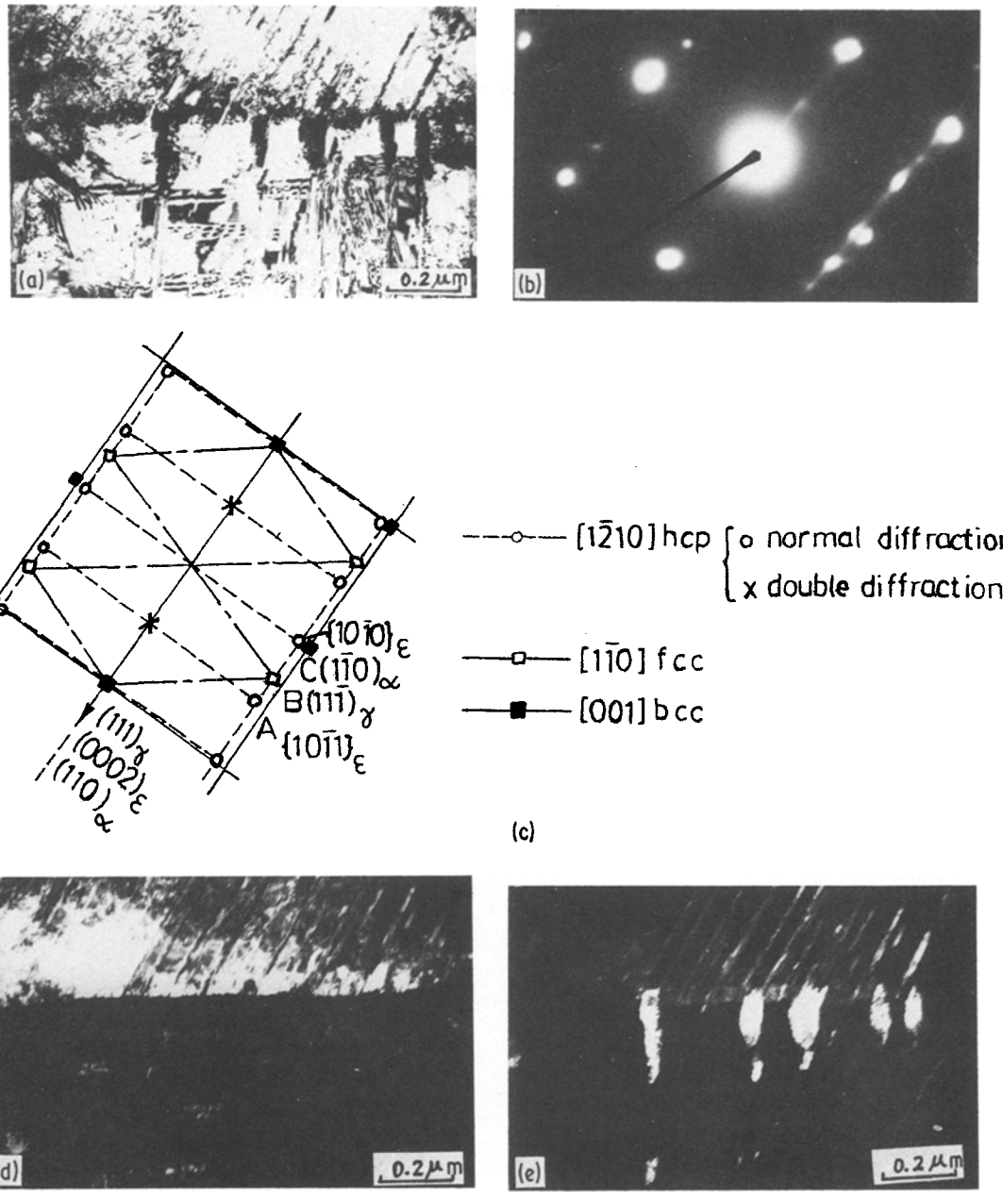

Figure 4 TEM microstructure of a specimen with 0% prior strain and 30% final strain: (a) bright-field image; (b) diffraction pattern taken at centre of (a); (c) indexed diffraction pattern; (d) dark-field image due to spot A; (e) dark-field image due to spot C.

final strain of 30%, also shows the existence of α martensite. Fig. 4b is a selected area diffraction pattern of the central area in Fig. 4a. The diffraction pattern is schematically drawn and indexed in Fig. 4c. Dark-field images by reflections due to A $[(1\,0\,\bar{1}\,1)_\epsilon]$ and C $[(1\,0\,\bar{1}\,0)_\epsilon$ and $(1\,\bar{1}\,0)_\alpha]$ were taken and are shown in Figs. 4d and e. Fig. 4d indicates that many ϵ platelets were formed after deformation to 30% thickness reduction at liquid-nitrogen temperature. Since the diffraction spots representing the α phase were always very close to ϵ spots, it was very difficult for us to take the dark-field image due to α spot reflection alone. Fig. 4e shows the dark-field image due to α and ϵ reflections. If we compare Fig. 4d with Fig. 4e, it is clear that the parallel platelets are the ϵ phase and

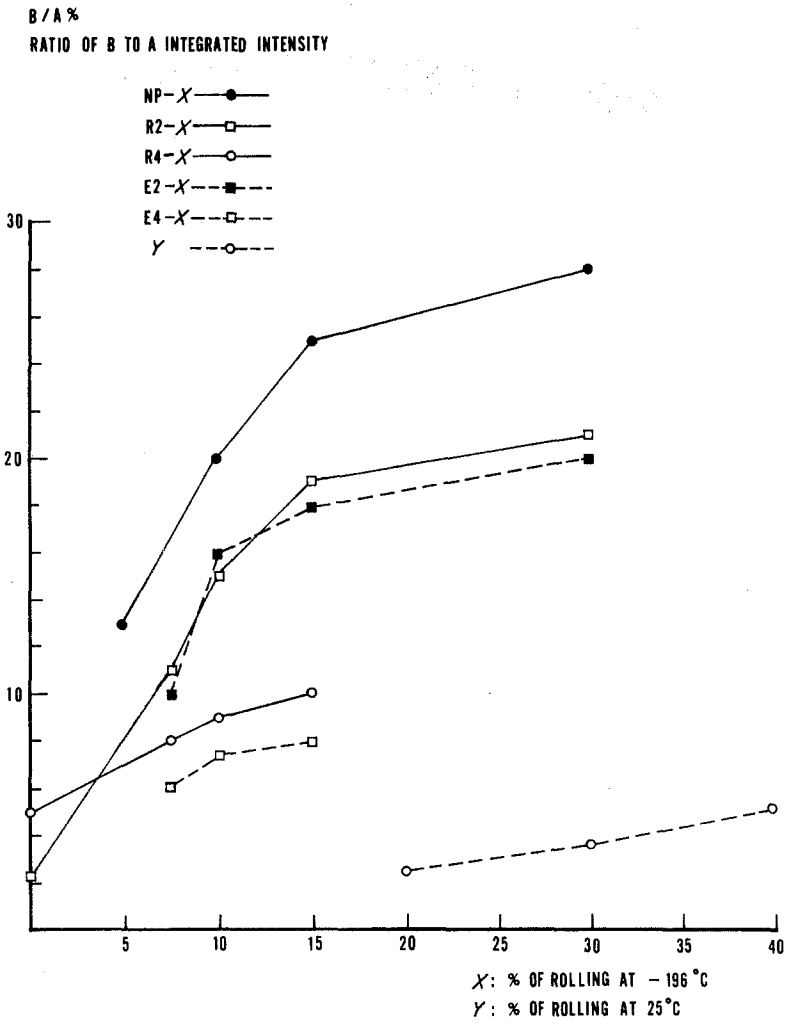

Figure 5 Volume fraction of martensite in specimens with different amounts of pre-strain and final strain. NP denotes no prior strain. R2 and R4 indicate 20% and 40% of prior strain at 25° C. E2 and E4 represent 20% and 40% of prior strain at 200° C.

the lath-like islands are the α phase. Also, the α phase was found predominantly at the intersections of ϵ bands with stacking faults, with grain boundaries, or with another ϵ band.

3.2. Pre-strain effect on austenite stability

The effect of pre-strain on martensite transformation was demonstrated in Figs. 2 and 5. As shown in Fig. 2, many peaks of different phases overlap each other, which made quantitative analysis difficult. The height of peak A is independent of the amount of pre-strain. This is reasonable because the intensity of this peak represents the volume fraction of total phases (γ, ϵ and α), which should be a constant (100%). This peak can be used as a basis for comparison. Peaks $(1\,0\,\bar{1}\,1)_\epsilon$ and $(2\,0\,0)_\alpha$ are very close to peaks $(2\,0\,0)_\gamma$ and $(1\,0\,\bar{1}\,2)_\epsilon$ respectively. Owing to the possibility of overlapping, they are no good for precise analysis of ϵ and α martensite transformation. Peak B, which is far away from neighbouring peaks, clearly represents the combination reflection of $(2\,1\,1)_\alpha$ and $(1\,0\,\bar{1}\,3)_\epsilon$ in which both α and ϵ are martensite. Thus, we calculated the ratio of the integrated intensity of peak B to that of peak A (B/A) to demonstrate the change in martensite ($\alpha + \epsilon$) transformation due to various pre-strains. The results are illustrated in Fig. 5. For the same amount of rolling at $-196°$ C, B/A decreased as the pre-strain was increased. The effect of pre-strain on martensite transformation was more pronounced in specimens pre-strained at 200° C

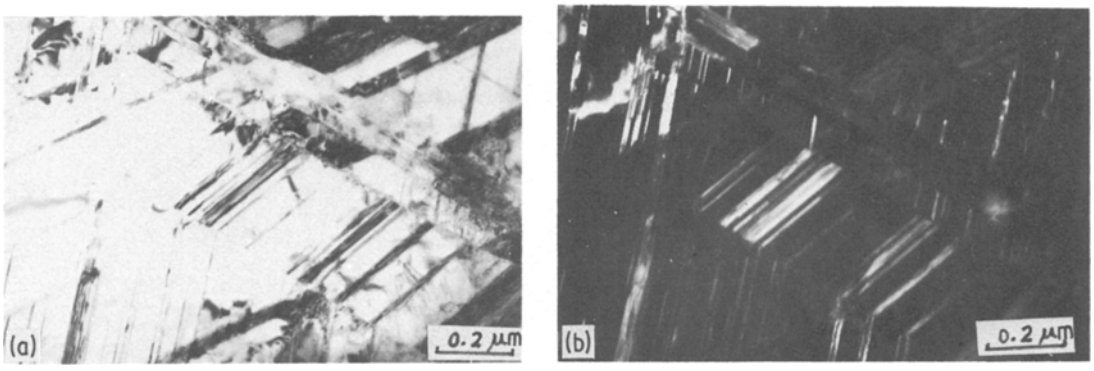

Figure 6 TEM microstructure of a specimen with 0% of prior strain and 15% of final strain: (a) bright-field image and (b) dark-field image of ϵ reflection.

than in specimens pre-strained at 25° C. The increased rate of ratio B/A decreased either as the pre-strain or final strain was increased. The effect of pre-strain on austenite stability was due to the fact that the growth of martensite was hindered by various substructures. Fig. 4 shows that the growth of martensite was hindered at grain boundaries and Fig. 6 indicates that martensite growth was hindered at twin boundaries.

3.3. Hardness and work hardening rate

The hardness data are illustrated in Fig. 7, which shows clear work hardening phenomena. The work hardening rate decreased as the amount of deformation at − 196° C was increased. The hardness tended to saturate after the specimen was rolled to a certain amount of reduction in thickness at − 196° C. The work hardening rate also decreased as the pre-strain was increased. Specimens without pre-strain possessed the lowest hardness and largest work hardening rate. The hardness and work hardening rate of various specimens can be explained in terms of their microstructures and will be discussed later.

4. Discussion

4.1. ϵ (h c p) and α (b c c) martensitic transformation

To explain the ϵ nucleation, many models were based on the overlapping of stacking faults on every second close-packed plane in γ. Bollmann [16] showed that, if two stacking faults intersect, a local stress field is produced at the intersection. This stress causes a new stacking fault on a $(1\,1\,1)_\gamma$ plane two atomic layers away from the original stacking fault. Thus, new stacking faults form in a regular order. One characteristic of this regular overlapping process is that, even in the early stages of ϵ formation, well defined diffraction spots of h c p appear. In most of our observations, well defined diffraction spots always accompanied ϵ formation. This indicates that ϵ formation in this study is mostly by a regular overlapping process. Occassionally, faulted ϵ was also found in our investigation, which is characteristic of the irregular overlapping process suggested by Fujita and Ueda [8]. The orientation relation, as shown in the diffraction pattern of Figs. 3b and c, is that $(1\,1\,1)_\gamma$ is parallel to $(0\,0\,0\,1)_\epsilon$ and $(1\,\bar{1}\,0)_\gamma$ is parallel to $(1\,\bar{2}\,1\,0)_\epsilon$, i.e. the close-packed planes and close-packed directions in the two structures are parallel.

In this investigation, the α phase was observed only when accompanied by the ϵ phase. The amount of ϵ phase was always much larger than the amount of α martensite. Besides, the α phase was found predominantly at the intersections of ϵ bands. All our experimental results indicated that the sequence of martensitic transformation in this Fe–Cr–Mn system was $\gamma \rightarrow \epsilon \rightarrow \alpha$.

4.2 Pre-strain effect on austenite stability

In this study, austenite stability depends on two factors: one is martensite nucleation, the other is growth of martensite. The growth of martensite may be hindered by substructures (subcells, subgrains and twins) introduced during the process of pre-strain or final strain. However, both pre-strain and final strain may introduce stacking faults, which favour martensite nucleation. At the early stage of final strain (straining 0 to 10% at − 196° C), martensite starts to nucleate and the growth of martensite is not yet hindered significantly by substructures (since the densities of

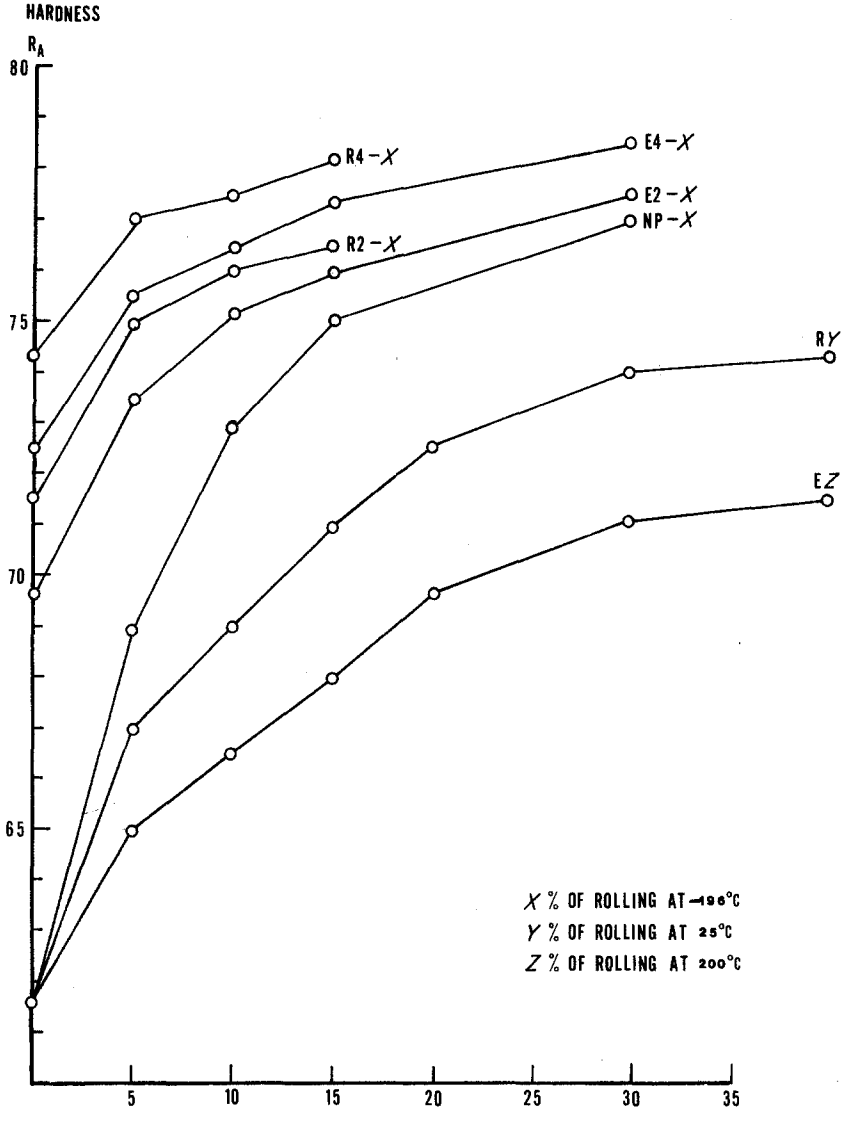

Figure 7 Correlation of hardness with pre-strain and final strain. Codes NP, E2, E4 R2 and R4 have been described in Fig. 5.

substructures and martensite are low). At the last stage of final strain (straining 15 to 30% at -196° C), the density of stacking faults starts to saturate such that martensite nucleation slows down, and the growth of martensite is considerably retarded (since the densities of substructures and martensite are higher). This explains why the slope of the transformation curves as shown in Fig. 5 decreased as the final strain was increased. The effect of pre-strain is to introduce a high density of substructures (as shown in Fig. 8), which retards martensite growth. The improvement of austenite stability by pre-strain is evident in this study.

The twin, dislocation cell and ϵ phase introduced during pre-strain at 25° C (Fig. 8a) may act as efficient obstacles to the growth of the ϵ phase during final straining. The substructures resulting from pre-strain at 200° C are mostly dislocation cells (Fig. 8b), which may also retard the growth of the ϵ phase. Because many stacking faults were produced in specimens by pre-strain at 25° C (which favoured ϵ phase nucleation), the effect of ϵ, twins and dislocation cells on austenite stabilization was counteracted by the effect of stacking faults on ϵ formation. This explains why the effect of austenite stability by pre-strain at 200° C was more significant than pre-strain at 25° C. The pre-strain can retard the nucleation and growth of

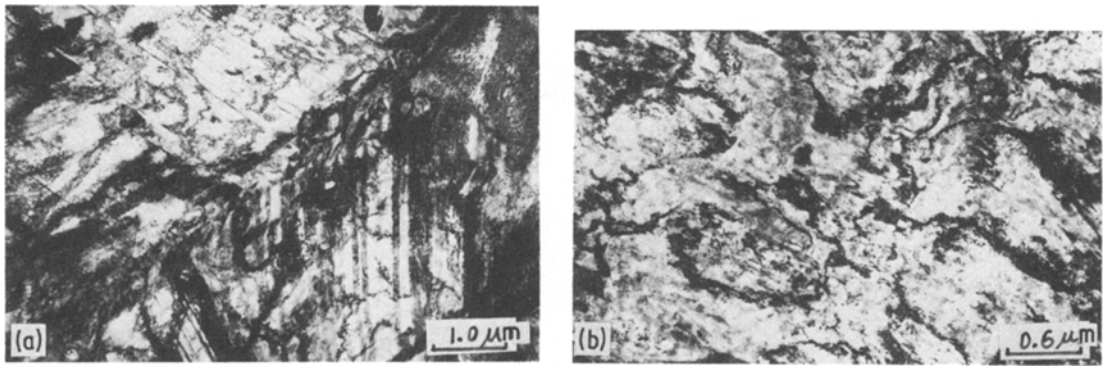

Figure 8 TEM microstructure of specimens: (a) specimen with 20% of prior strain at 25° C and 0% of final strain; (b) specimen with 20% of prior strain at 200° C and 0% of final strain.

the α phase since α formation depends on ϵ and the ϵ phase decreases significantly through pre-strain treatment.

4.3. Hardness and work hardening rate

The substructures introduced after deformation at 200, 25 and $-196°$ C were very different from each other. Dislocations and dislocation cells were predominantly observed in specimens after deformation at 200° C (Fig. 8b). Besides dislocation cells, large amounts of mechanical twins and stacking faults and small amounts of ϵ were introduced after deformation at room temperature (Fig. 8a). Larger amounts of stacking faults and ϵ phase were formed by deformation at $-196°$ C (Fig. 3). These differences in substructure introduced by deformation at different temperatures can be rationalized in terms of stacking fault energy [10, 17]. Therefore, the present observation suggests a strong temperature dependence of stacking fault energy. The lower work hardening rate by deformation at 200° C is due to the fact that only dislocation is active in the role of work hardening. The work hardening rate increased as mechanical twins and stacking faults were introduced during deformation at 25° C. The enormous work hardening rate by deformation at $-196°$ C was mainly due to the formation of ϵ and α martensite.

After pre-strain and then rolling at $-196°$ C, the work hardening was mainly due to ϵ phase formation. After about 15% of rolling at $\sim 196°$ C, the work hardening rate decreased because the increase of ϵ phase formation slowed down. As the amount of deformation increases, the density of substructures also increases, and the growth of the ϵ phase becomes more and more difficult. Thus, after a certain amount of deformation, the ϵ phase will approach a saturation value, and the work hardening rate decreases.

5. Conclusions

1. The annealed Fe–Cr–Mn alloy investigated in this study possesses a full austenite phase with high stability. M_s is below $-196°$ C and M_d is above 25° C.

2. Plates of hcp phase (ϵ) are formed in Fe–Cr–Mn alloy predominantly by regular overlapping of stacking faults. Plane $(1\,1\,1)_\gamma$ is parallel to $(0\,0\,0\,1)_\epsilon$ and direction $(1\,\bar{1}\,0)_\gamma$ is parallel to $(1\,\bar{2}\,1\,0)_\epsilon$.

3. The martensite transformation sequence is $\gamma \rightarrow \epsilon \rightarrow \alpha$. Nucleation of the α phase mainly occurs at the intersection of two ϵ bands or at the intersection of the ϵ band and twin or grain boundaries.

4. Austenite stability is improved by pre-strain at 25° C or 200° C. Pre-strain at 200° C has a larger effect on austenite stability than does pre-strain at 25° C. The mechanisms are discussed in terms of the substructures introduced during straining.

5. The work hardening rate depends on the amount of pre-strain and final strain. The correlation between work hardening rate and the substructure introduced during pre-straining and final straining is discussed.

References

1. W. Y. C. CHEN and J. R. STEPHENS, *Corrosion* **35** (1979) 443.
2. C. M. HSIAO and E. J. DULIS, *Trans. ASM* **52** (1960) 855.
3. J. N. KASS, W. L. BELL, M. T. WANG and J. BOBICK, *Metall. Trans.* **10A** (1979) 715.
4. D. J. CHAKRABARTI, *ibid.* **8B** (1977) 121.

5. D. J. SCHMATZ, *Trans. ASM* **52** (1960) 898.
6. C. M. WANG, H. J. LAI, M. T. JAHN, C. T. HU and J. HEH, "Specialty Steels and Hard Materials" (Pergamon Press, 1982) p. 221.
7. R. WANG and F. H. BECK, *Metal Prog.* March (1983) 72.
8. H. FUJITA and S. UEDA, *Acta Metall.* **20** (1972) 759.
9. J. R. STRIFE, M. J. CARR and G. S. ANSELL, *Metall. Trans.* **8A** (1977) 1471.
10. L. REMY and A. PINEAU, *Mater. Sci. Eng.* **28** (1977) 99.
11. P. L. MANGONON, Jr and G. THOMAS, *Metall. Trans.* **1** (1970) 1577.
12. G. B. OLSON and M. COHEN, *ibid.* **6A** (1975) 791.
13. J. DASH and H. M. OTTE, *Acta Metall.* **11** (1963) 1169.
14. P. M. KELLY, *ibid.* **13** (1965) 635.
15. K. SIPOS, L. REMY and A. PINEAU, *Metall. Trans.* **7A** (1976) 857.
16. W. BOLLMANN, *Acta Metall.* **9** (1961) 972.
17. H. SUZUKI and C. S. BARRETT, *ibid.* **6** (1958) 156.

Received 16 January
and accepted 31 July 1984